Dynamics of submarine groundwater discharge and freshwater-seawater interface

Makoto Taniguchi
Research Institute for Humanity and Nature, Kamigyo-ku, Japan

Tomotoshi Ishitobi
Nara University of Education, Takabatake, Japan

Jun Shimada
Department of Earth Sciences, Kumamoto University, Kurokami, Japan

Received 17 February 2005; revised 22 April 2005; accepted 13 October 2005; published 20 January 2006.

[1] Relationships between submarine groundwater discharge (SGD) and the freshwater-saltwater interface are evaluated by continuous measurements of SGD rates, conductivity and temperature of SGD, and resistivity measurements across the coastal aquifer. Our measurements show that the processes of SGD differ between the offshore and nearshore environments. SGD and submarine fresh groundwater discharge (SFGD) rates were largest just landward of the saltwater-freshwater interface. SGD variations landward the saltwater-freshwater interface had negative correlations with tidal variations, because of the connections of terrestrial groundwater in the land and the ocean. SGD in the nearshore can be explained mainly by connections of terrestrial groundwater, while offshore SGD rate is controlled mostly by oceanic process such as recirculated saline groundwater discharge.

Citation: Taniguchi, M., T. Ishitobi, and J. Shimada (2006), Dynamics of submarine groundwater discharge and freshwater-seawater interface, *J. Geophys. Res.*, *111*, C01008, doi:10.1029/2005JC002924.

1. Introduction

[2] Submarine groundwater discharge (SGD) has been recognized recently as a significant water and material pathway from land to ocean [*Moore*, 1996; *Burnett*, 1999; *Burnett et al.*, 2001], and has stimulated studies from both hydrological and coastal oceanographic communities [*Li et al.*, 1999; *Hussain et al.*, 1999; *Smith and Zawadzki*, 2003; *Burnett et al.*, 2003; *Chanton et al.*, 2003]. Recent field work revealed that SGD contains submarine fresh groundwater discharge (SFGD) and recirculated saline groundwater discharge (RSGD) [*Gallagher et al.*, 1996; *Li et al.*, 1999; *Taniguchi et al.*, 2002, 2003a], and that there are tidal effects on SGD [*Taniguchi*, 2002; *Kim and Hwang*, 2002]. Because SGD is difficult to detect and quantify, there are still many uncertainties in understanding the subsurface processes.

[3] It is important for evaluating material transport from land to ocean by SGD to separate SGD into SFGD and RSGD. *Taniguchi and Iwakawa* [2004] compared observed SGD by automated seepage meter with the calculated terrestrial SFGD. The SFGD rate was estimated by multiplying the observed hydraulic gradients between sea level and groundwater level, and the estimated hydraulic conductivity under the assumption of the Darcy's law. They found the ratio of SFGD to total SGD ranged from 1% to 29% in Osaka bay, Japan. Ratios of SFGD to SGD were also estimated in other studies to be 35% using seepage meters and salinity measurements by *Gallagher et al.* [1996], 10% using ^{222}Rn and ^{226}Ra measurements by *Hussain et al.* [1999], and 4% using numerical simulations by *Li et al.* [1999]. However, temporal and spatial variations of SFGD/SGD ratios and process of the variations are still not clear.

[4] Saltwater-freshwater interfaces have been intensively studied in hydrological communities for many years, because saltwater intrusion due to excessive groundwater mining is a serious problem for water resources in coastal areas. *Badon-Ghyben* [1889] and *Herzberg* [1901] first studied the phenomenon of seawater intrusion into groundwater aquifers in coastal regions. Many numerical simulations and related works attempt to evaluate mechanisms governing this process [e.g., *Segol and Pinder*, 1976; *Freeze and Cherry*, 1979; *Huyakorn et al.*, 1987]. Though SGD and seawater intrusion processes may seem to be exactly opposite, saltwater intrusion into coastal aquifers and SGD are entirely complementary processes. The extent of SGD or freshwater-saltwater interface at a given location is essentially an issue of balance between hydraulic and density gradients in groundwater and seawater along a transect perpendicular to the shoreline. However, there are few studies on both SGD and saltwater-freshwater interface in the coastal areas. The purposes of this study are to evaluate (1) the temporal and spatial variations of SGD and how SGD relates to the freshwater-saltwater interface, (2) relationships between SFGD and RSGD, and (3) effects salt-

0148-0227/06/2005JC002924

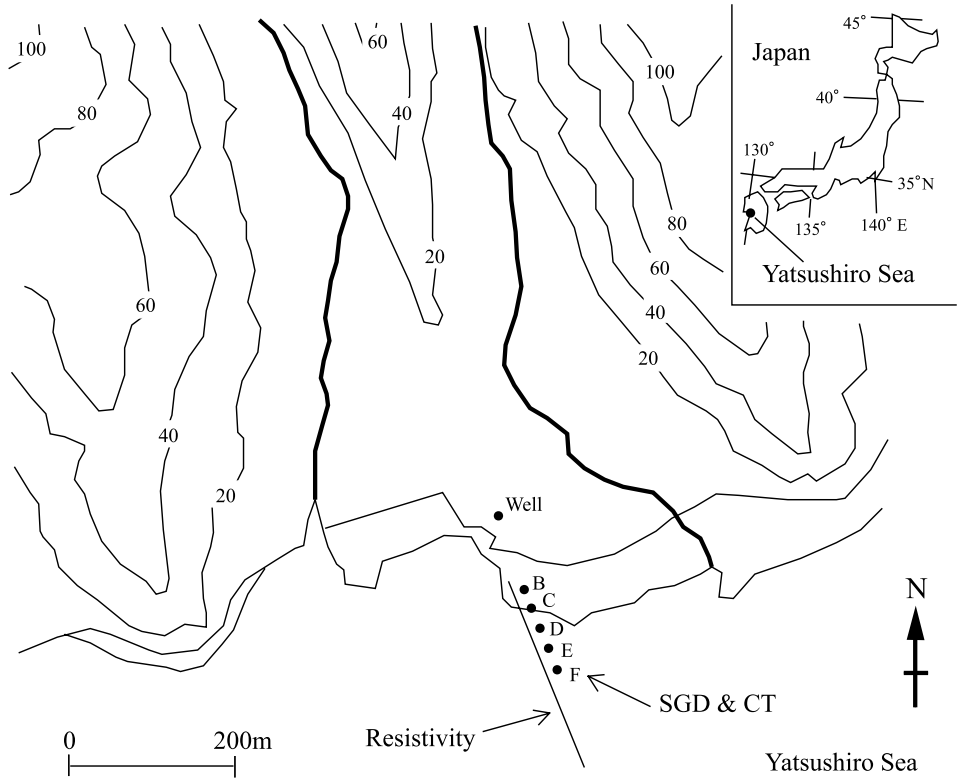

Figure 1. Location of the study area. The elevations are shown in meters, and the dark lines show the rivers. The shoreline shows the location of the coast at low tide.

water-freshwater interface variations have on SFGD and RSGD.

2. Study Area and Methods

[5] Study area is a coastal zone of Yatsushiro Sea in Kyushu island, Japan (Figure 1). Aquifers in this study area consist of permeable quaternary volcanic rocks (andesite lava and tuff breccia) and pyroclastic flow deposits. The basin area is 4.5 km^2, and the length of the basin from the top (elevation is 400 m above sea level) to the coast is 4 km. The annual precipitation is about 1840 mm yr^{-1}, and average annual air temperature is about 16.7°C. The Yatsushiro Sea is an inland sea, and the average of tidal change is from 3 to 5 m.

[6] Automated seepage meters have been recently developed using heat pulse method [*Taniguchi and Fukuo*, 1993, 1996; *Krupa et al.*, 1998], ultrasonic measurements [*Paulsen et al.*, 2001], electromagnetic methods [*Rosenberry and Morin*, 2004] and continuous heat flow measurements [*Taniguchi and Iwakawa*, 2001; *Taniguchi et al.*, 2003a]. Five continuous heat-type automated seepage meters were located at 30, 60, 90, 120, and 150 m distance offshore from the coastal line at high tide in Yatsushiro (Figure 1). The seepage meters B and C are located between high tide coast and low tide coast. The automated seepage meter is based on the effect of heat convection due to water flow by measuring the temperature gradient of the water flowing between the downstream and upstream positions in a horizontal flow tube with a diameter of 1.3 cm, which is connected to the chamber. The principle of the automated seepage meter is described in detail by *Taniguchi and Iwakawa* [2001] and *Taniguchi et al.* [2003a]. The average depth of the seawater at the location of the seepage meter is 0.9, 1.2, 1.5, 1.8, and 2.0 m at B, C, D, E, and F, respectively. The area of the chamber with the diameter of 0.57 m for the seepage meter is 0.255 m^2. Although *Shinn et al.* [2002] criticized the seepage meter measurements, recent field evaluations of the SGD using seepage meters showed that consistent and reliable results can be obtained even in the heterogeneous situations if one accounts for the potential problems [*Cable et al.*, 1997]. The water in the chamber can be replaced within one day if seepage rate is larger than 10^{-7} m s^{-1}. Measurements of SGD using the continuous heat type automated seepage meter have been done every 10 minutes from 2 to 7 August 2003. Tidal (sea) levels were recorded every 10 minutes at F using a pressure transducer which was attached to the outside of the camber of the seepage meter. The groundwater levels in a well were also measured continuously every 10 min at 80 m inland from the coast. The diameter and depth of the well is 0.73 m and 18.5 m, respectively. Conductivities and temperatures of waters within the chambers were also measured continuously by conductivity-temperature-depth (CTD) sensors (DIK 603A CTD, Daiki Rika Kogyo, Co., Ltd.) which were installed in the chamber of the five seepage meters.

[7] Tidal sea level, groundwater level and precipitation during the study are shown in Figure 2. The amplitude of the semidiurnal sea level change ranges from 140 cm on 3 August to 70 cm on 6 August with neap tide. Resistivity under the seabed and land surface at the transect line which is perpendicular to the coast (Figure 1) were measured by Sting R1 IP/Swift (American Geophysical Instrument).

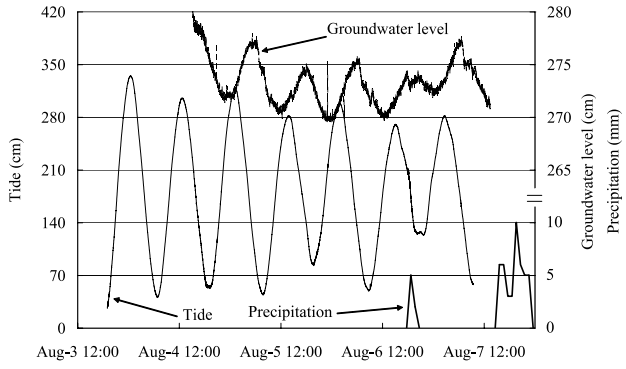

Figure 2. Changes in sea level, groundwater level, and precipitation.

There are 28 probes along the 270-m transect (interval length between probes was 10 m). The Wenner method and RES2DINV version 3.50 (Geotomo Software) were used for the resistivity analyses. The cross-sectional result of resistivity measurements along the transect line at the lowest tide on 18 September 2003 (one-and-a-half months after of the seepage measurements) is shown in Figure 3. The darker color shows fresher water (higher resistivity), and lighter color shows saltier water (lower resistivity). The direction of the saltwater-freshwater interface is different from the traditional Ghyben-Herzberg's one (the interface becomes shallower toward offshore [*Ghyben*, 1899; *Herzberg*, 1901]), because Figure 3 only shows the resistivity of the pore water at shallower than 50 m depth. As can been seen from Figure 3, seepage meters B, C, and D are located at relatively fresh seepage area; on the other hand, E and F are located in a relatively saltier area.

3. Temporal and Spatial Variations of SGD

[8] Temporal variations of SGD using automated seepage meters are shown in Figure 4a at B, C, and D, and in Figure 4b at E and F. There are gaps in the SGD data, because automated seepage meters B and C were sometimes exposed at low tide. As can be seen from Figure 4a and Figure 4b, semidiurnal variations of SGD were found at all locations except some periods at location E. The time delays of SGD variations between B-C-D and E-F were also found. The SGD variations at E and F are a couple of hours behind of SGD variations at B, C, and D. The amplitude of SGD variations ranges from 2×10^{-6} m s^{-1} (17.3 cm/day) at E and D, to 12×10^{-6} m s^{-1} (103.7 cm/day) at C and F. The increase of SGD at the evening of 6 August may be caused by precipitation (Figure 2). Total precipitation from 1900 local time to 2100 local time on 6 August was 7 mm. The relationship between SGD and precipitation was discussed in other areas such as Osaka bay, Japan, by *Taniguchi et al.* [2002]; however, the relationship is not fully understood.

[9] Spatial variations of SGD at transect line from B to F (Figure 1) are shown in Figure 5. The x axis shows the distance from the coast at the high tide. SGD rates sometimes have a general tendency of decreasing with distance away from the coast, which is consistent with theory [*McBride and Pfannkuch*, 1975], and observation in lakes [*Lee*, 1977; *Fellows and Brezonik*, 1980; *Shaw and Prepas*, 1990] and marine systems [*Bokuniewicz*, 1980], but not always the case [*Cable et al.*, 1997; *Taniguchi et al.*, 2003b]. The seepage rates at C show the maximum value, perhaps because of preferential flow caused by channeling due to high permeability or upward flow along the saltwater-freshwater interface due to regional groundwater discharge [*Freeze and Cherry*, 1979].

4. Changes in Conductivity and Temperature of SGD

[10] Changes in electric conductivities of SGD are shown in Figure 6. The tendency of the changes in conductivity was different between B-C-D and E-F. Semi-diurnal variations of the conductivities were found at E and F, but not at B, C, and D. The general trend of decrease in conductivity at C and D may be the change of the component of seepaged water from spring tide (31 July) to neap tide (7 August, Figure 2). Lager conductivity of SGD during spring tide is caused by larger RSGD among SGD, because higher amplitude of tidal change causes more recirculated seawater discharge. Therefore the tidal pumping is the cause of the RSGD. There are other potential causes for RSGD

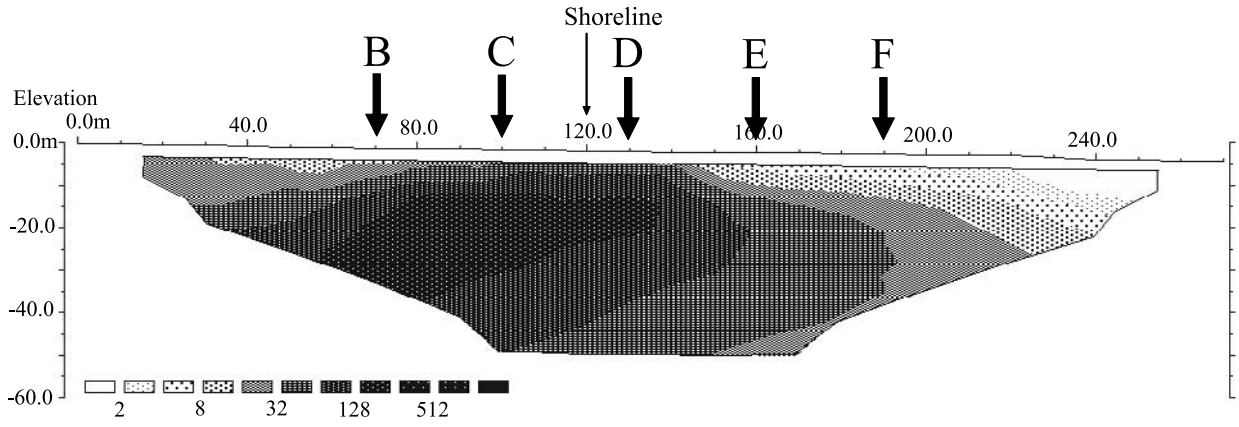

Figure 3. Resistivity cross section in a 250-m-long transect perpendicular to the coast with the low-tide mark at 120 m. The y axis shows the elevation.

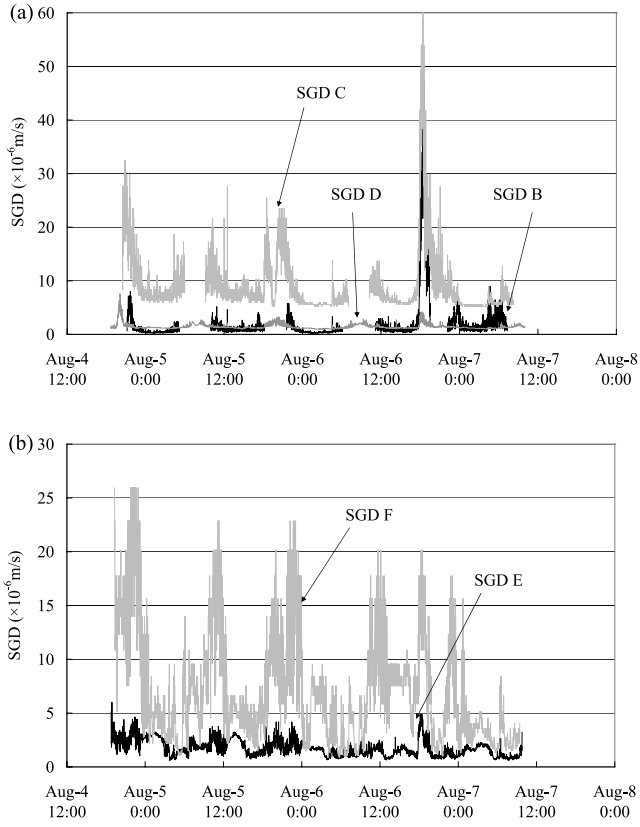

Figure 4. Changes in SGD rate at (a) B, C and D and (b) E and F.

such as wave setup [*Li et al.*, 1999]; however, the main cause of larger conductivity of SGD may be the tidal pumping. On the other hand, the conductivity of SGD at location B does not show a decrease trend from spring to neap tide or semidiurnal change unlike C and D. The reason for the lowest conductivity of SGD at location C is that since the place is just landward of the freshwater-saltwater interface (Figure 3), the larger freshwater discharge is expected. Changes in temperature of SGD and seawater are shown in Figure 7. As with changes in conductivity, the tendency of the changes in temperature is different between B-C-D and E-F. The temperature change amplitude was about 0.5°C at B, C, and D, however the amplitude at E and

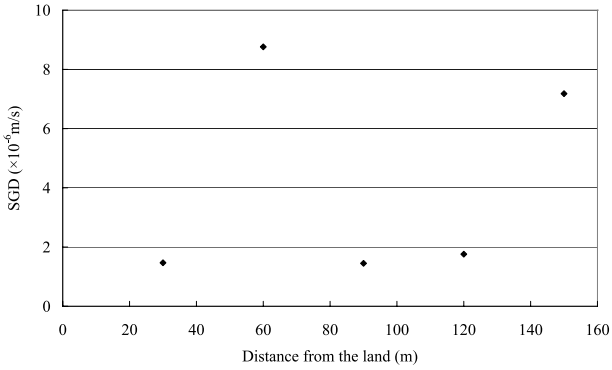

Figure 5. Relationship between average SGD and the distance from the coast. The *x* axis shows the distance from the coast at high tide.

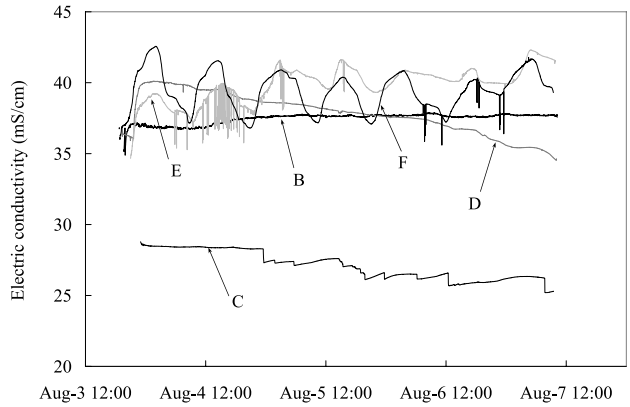

Figure 6. Temporal changes in conductivity of SGD.

F was more than 1.0°C as well as seawater. The amplitudes of groundwater and air temperature at a well (Figure 1) were 0.11° and 11.4°C, respectively.

[11] Figure 8 shows the relationships between electric conductivity and temperature of SGD, and the distance from the coast. As can be seen from Figure 8, the conductivity and temperature of SGD increases with the distance from the coast, with the spike at C, where SGD rate was the maximum. The averages of temperature and conductivity of seawater during the observation period were 29.96°C, and 42.57 mS cm^{-1}, respectively.

[12] As there are two groups (1, B-C-D, and 2, E-F) from the variations of conductivity and temperature of SGD, the relationships between SGD rate and tidal level, temperature and conductivity of SGD are examined in detail and shown in Figure 9a for D (group 1) and Figure 9b for F (group 2). SGD at D has negative correlations with tidal level, and temperature of SGD (Figure 9a), but there are time lags between SGD at F and other three parameters (Figure 9b).

[13] Correlation analyses have been made in order to evaluate the time correlations between SGD, tidal level, conductivity, and temperature for all locations. Analyses have been done with one hour time varied between two values. Correlation coefficients between (Figure 10a) SGD and tidal level, (Figure 10b) SGD and conductivity, and (Figure 10c) SGD and temperature for five locations are shown in Figure 10. The best correlations (highest absolute values of correlation coefficient) were found at B, C, and D when the SGD was 6 hours behind (or 6 hours ahead) the

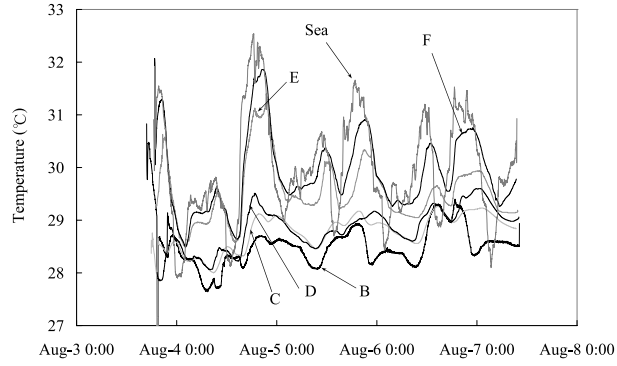

Figure 7. Temporal changes in temperature of SGD.

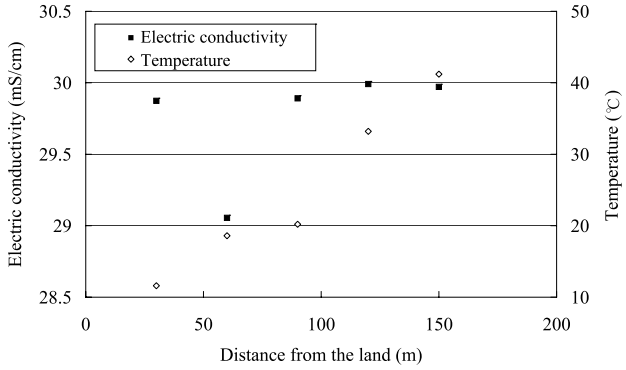

Figure 8. Spatial variations of averages of SGD conductivity and temperature with distance from the coast.

tidal level change. This means that the SGD is the largest with the lowest sea level. On the other hand, the maximum coefficients were found at E and F when the SGD was 9 hours behind (or 3 hours ahead) tidal change. This means maximum SGD occurs three hours after the maximum hydraulic gradient because the change in groundwater level is negligible compared to the sea level change (i.e., the hydraulic gradient between land and ocean is mainly determined by the sea level change). Regarding the relationships between SGD and conductivity (Figure 10b) and between SGD and temperature (Figure 10c), semidiurnal variations of correlation coefficients were only found at group 2 (E and F). No significant variations of correlation coefficients were found at group 1 (B, C, and D). Therefore

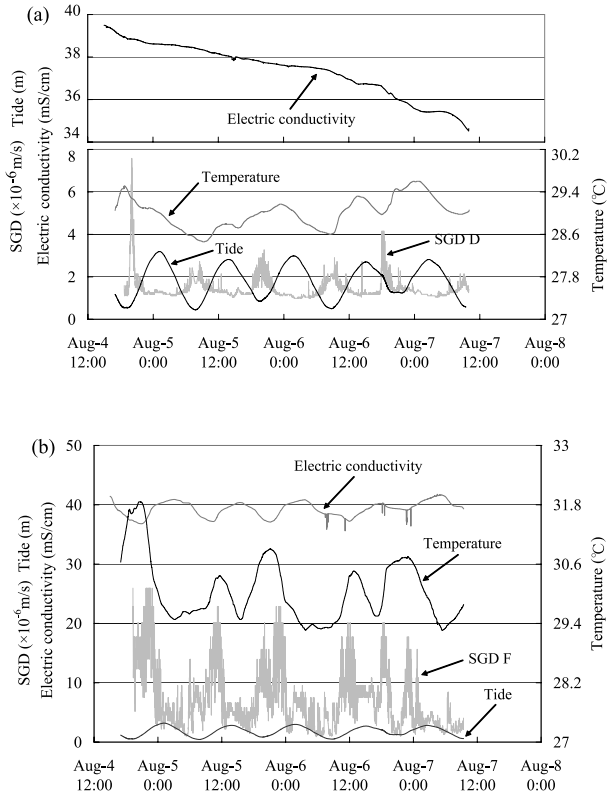

Figure 9. Relationships between SGD, tide, temperature, and conductivity at (a) D and (b) F.

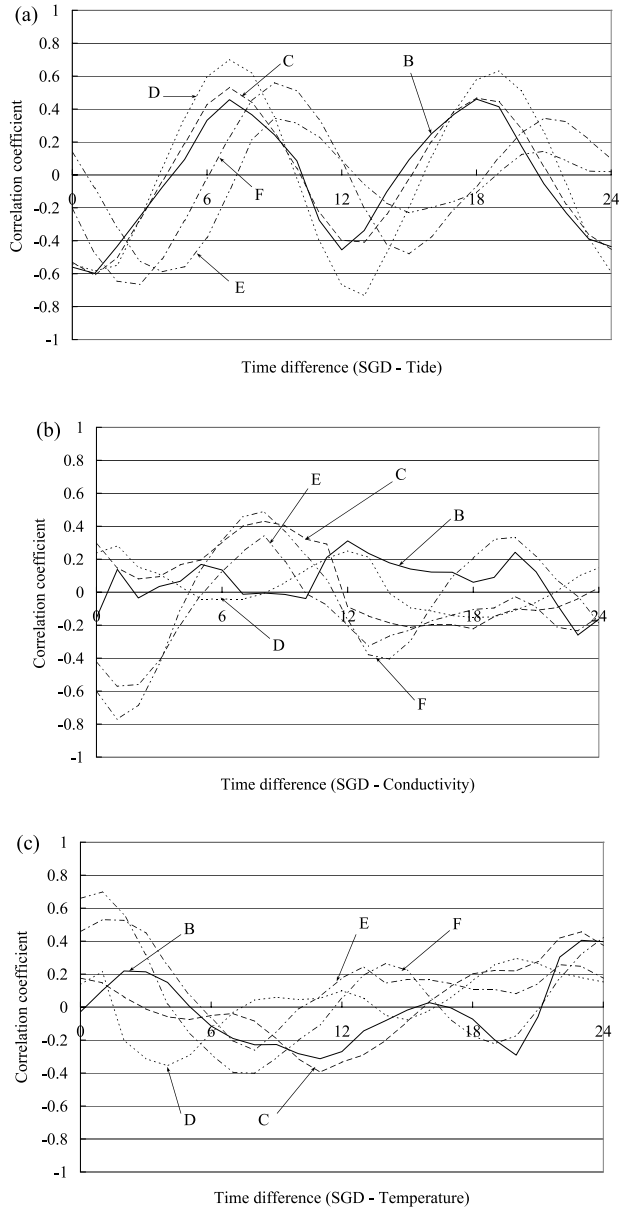

Figure 10. Correlation coefficients between SGD and (a) tide, (b) conductivity, and (c) temperature.

SGD at group 2 which is far from the coast is strongly affected by the seawater related to the tidal changes with semidiurnal variations. This means that SGD at group 2 (E and F) is strongly controlled by tidal pumping.

5. Separations of SGD

[14] In order to separate SGD into terrestrial fresh groundwater discharge and recirculated saline water, analyses of water and material budgets using two end-members have been made. Water balance and material balance equations at the seabed are described as follows:

$$\mathrm{SGD} = \mathrm{SFGD} + \mathrm{RSGD} \tag{1}$$

$$C_{\mathrm{SGD}} \times \mathrm{SGD} = C_{\mathrm{SFGD}} \times \mathrm{SFGD} + C_{\mathrm{RSGD}} \times \mathrm{RSGD}, \tag{2}$$

Table 1. Separations of SGD into SFGD and RSGD

	Electric Conductivity, mS cm^{-1}	Observed SGD, $\times 10^{-6}$ m s^{-1}	SFGD, $\times 10^{-6}$ m s^{-1}	RSGD, $\times 10^{-6}$ m s^{-1}	SFGD/SGD
B	37.47	2.087	0.245	1.842	0.117
C	27.10	9.175	3.457	5.718	0.377
D	37.82	1.452	0.182	1.270	0.125
E	39.82	1.758	0.107	1.651	0.061
F	39.42	7.176	0.675	6.501	0.094

where C_{SGD}, C_{SFGD}, and C_{RSGD} are conductivities of the water that compose the SGD, SFGD and RSGD, respectively. Conductivities of the SGD at each location as C_{SGD}, the fresh terrestrial groundwater at location W as one end-member of C_{SFGD}, and seawater as another end-member of C_{RSGD} were used to separate SGD into SFGD and RSGD.

[15] According to the changes in conductivity of the SGD (Figure 6), the averaged SGD conductivity was 37.47, 27.1, 37.82, 39.82, and 39.42 mS cm^{-1} at B, C, D, E, and F, respectively. Incorporating average SGD of 2.087×10^{-6} m s^{-1} (18.0 cm/day), 9.175×10^{-6} m s^{-1} (79.3 cm/day), 1.452×10^{-6} m s^{-1} (12.6 cm/day), 1.758×10^{-6} m s^{-1} (15.2 cm/day), and 7.176×10^{-6} m s^{-1} (62.0 cm/day) at B, C, D, E, and F, C_{SGD} (Table 1), C_{SFGD} of 0.160 mS cm^{-1}, and C_{RSGD} of 54.39 mS cm^{-1} into equations (1) and (2), SFGD and RSGD were calculated, and shown in Table 1. As can be seen from Table 1, the ratio of SFGD to SGD was largest at C where SGD rate was maximum.

[16] Figure 11 shows the changes of the ratio of SFGD to SGD at five locations. Again, there are two groups for the changes in the ratio of SFGD to SGD. The ratio at E and F have semidiurnal variations, but not at B, C, and D. This is attributed to the changes of RSGD by tidal effects on SGD at E and F. This analysis is based on a simple chemical budget calculation using two end-members (fresh groundwater and seawater). The processes of the mixture of SFGD and RSGD are still not clear, and further studies are needed.

6. Simulations of SGD Rate

[17] Offshore seepage rates from surficial unconfined aquifers have been described by an exponentially decreasing function with the distance from the coast [*McBride and Pfannkuch*, 1975]. They investigated the distribution of groundwater seepage rate through lake beds using numerical models. *Bokuniewicz* [1992] developed an analytical solution for SFGD from steady state Richards' equation instead of exponential function as follows:

$$q = (K_v i/\pi k)\ln[\coth(\pi x k/4l)], \quad (3)$$

where i is hydraulic gradient, x is the horizontal distance from the coast, k is the square root of the ratio of the vertical hydraulic conductivity (K_v) to the horizontal hydraulic conductivity (K_h), and l is aquifer thickness.

[18] To simulate the change of SFGD (terrestrial freshwater component of groundwater discharge) rate from land to the ocean, analyses using equation (3) have been made. Observed and estimated values of k, i, and l (Table 2) are incorporated into the equation (5), then the independent parameter, x (the distance from the coast to each seepage meter), was used for the simulations by

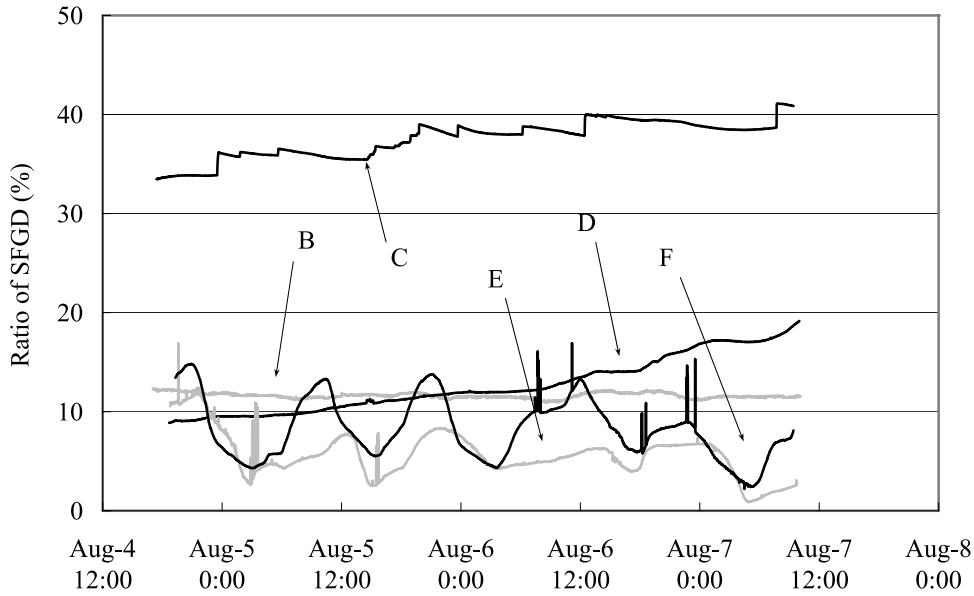

Figure 11. Temporal variations in the fresh groundwater discharge (terrestrial source).

Table 2. Parameters Used for SGD Simulations

	Kv, cm/s	k	i	L, m
B	0.0029	0.13	0.001	50
C	0.0579	0.13	0.001	50
D	0.0035	0.13	0.001	50
E	0.0002	0.13	0.001	50
F	0.0012	0.13	0.001	50

adjusting average-calculated SFGD to average-observed SFGD. The k is assumed to be 0.13 from the literature [*Shimada et al.*, 2003]. Figure 12 shows the calculated SFGD changes at B, C, D, E, and F with best fitted K_v which are shown in Table 2. As can be seen from Figure 12, SFGD at B, C, and D are well simulated, however not at E and F. Therefore SGD in the nearshore can be explained mainly by connections of terrestrial groundwater (SFGD), while offshore SGD rate is controlled mostly by oceanic process such as recirculated saline groundwater discharge. Wide range of the hydraulic conductivity in this study area was confirmed by other study [*Shimada et al.*, 2003].

7. Relationships Between SGD and Freshwater-Saltwater Interface

[19] As can be seen from Figure 3, seepage meters B, C, and D are located at relatively fresher seepage area which is shown as darker color in Figure 3, on the other hand, E and F are located in a relatively saltier area which is shown as

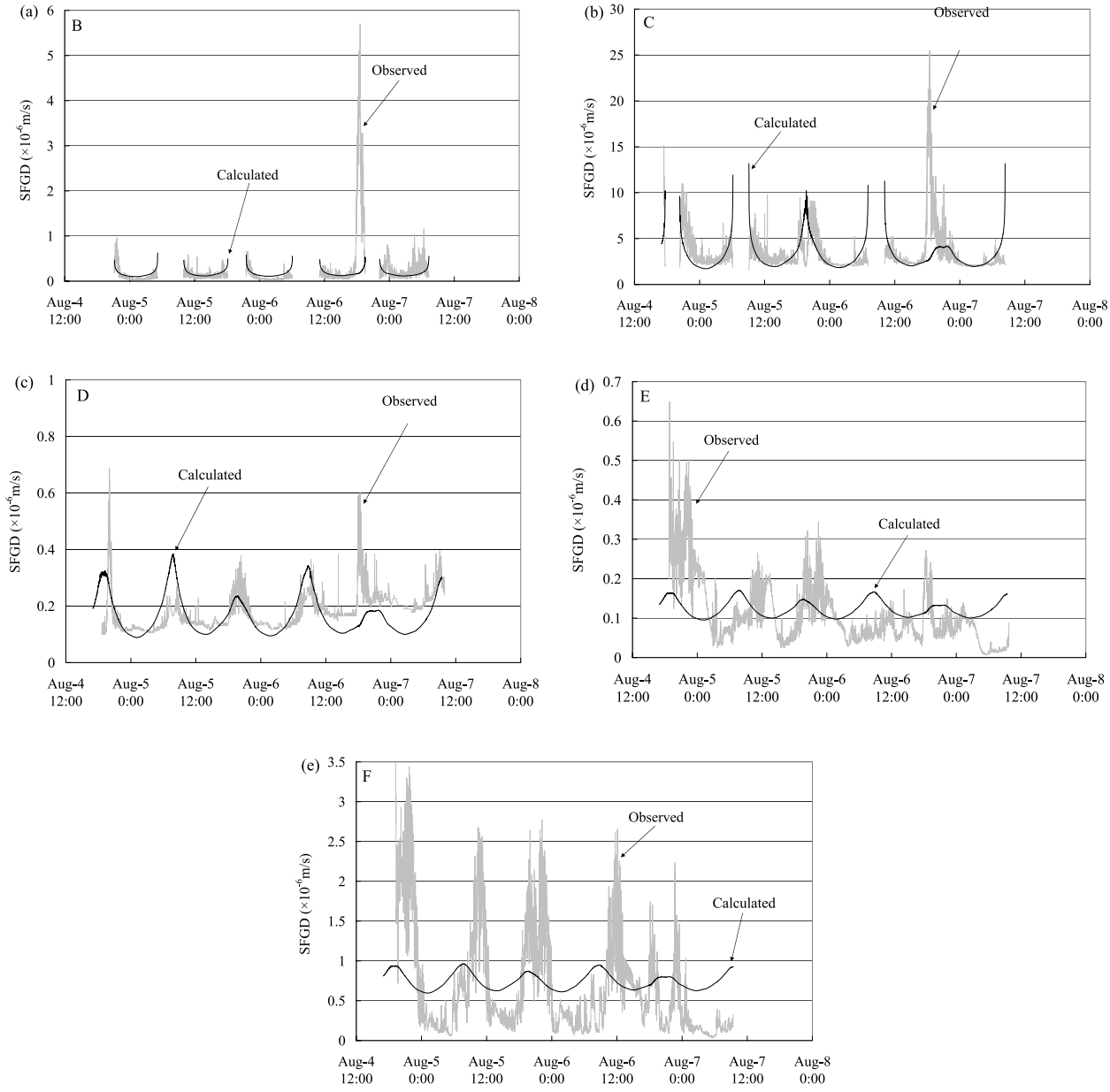

Figure 12. Comparisons between observed and calculated SFGD at (a) B, (b) C, (c) D, (d) E, and (e) F.

lighter color. According to laboratory experiments to evaluate the conductivity from resistivity for the sand of the study area, 30 ohm m of resistivity corresponds to the 10 mS cm^{-1} of conductivity ($Y = 423.5\ X^{-1.102}$; Y = resistivity, X = conductivity). The freshwater-saltwater interface is not usually sharp, but has a transient zone. Although we cannot define the location of the sharp interface, we can see the fresher water seepage face at B, C, and D. On the other hand, the locations E and F may be seaward of the freshwater-saltwater interface.

[20] According to the results of correlation analyses (Figure 10) and simulations using equation (3) (Figure 12), SGD processes are divided into two groups; 1 (B, C, and D) and 2 (E and F). Group 1 is located landward of the freshwater-saltwater interface and group 2 is located seaward of the interface. The terrestrial fresh groundwater discharge is the main factor at the locations landward the freshwater-saltwater interface. On the other hand, recirculated salt water is the main factor at the locations seaward of the interface. The process of SGD at the location B which is the closest to the coast, is a little more complicated, because resistivity (Figure 3) and SFGD/SGD ratio (Table 1) at B is the same level as those of offshore. This may be caused by the other effect such as wave setup which was discussed by *Li et al.* [1999].

8. Conclusions

[21] The main conclusions of this study are as follows.

[22] 1. SGD has semidiurnal variations and was largest just landward of the saltwater-freshwater interface. SGD variations within the saltwater-freshwater interface had negative correlations with tidal variations, because of the connections of terrestrial groundwater on the land and the ocean. Separation of SGD into SFGD and RSGD revealed than fresh terrestrial groundwater discharge was largest just landward of the saltwater-freshwater interface. Therefore this can be caused by the upward flow of terrestrial fresh groundwater discharge along the interface.

[23] 2. Electric conductivity of SGD seaward of the saltwater-freshwater interface was higher with semidiurnal variations than those landward of the interface which did not show the variations. Amplitude of SGD temperature variations were larger seaward of the interface than those landward of the interface, because the temperature variation of seawater is larger than that of groundwater. The ratio of SFGD to SGD landward of the saltwater-freshwater interface was higher without variation than those seaward of the interface which show the semidiurnal variations.

[24] 3. SFGD was simulated by terrestrial groundwater discharge model based on the function of the distance from the coast, but this model did not represent the offshore sites well. The processes of SGD differ between seaward and landward of the saltwater-freshwater interface. SGD landward of the interface can be explained mainly by connections of terrestrial groundwater, however, SGD seaward of the interface is controlled mostly by oceanic process such as recirculated saline groundwater discharge.

[25] **Acknowledgments.** The authors are grateful to W. C. Burnett, Florida State of University, and anonymous reviewers for critical reading and improvement of the manuscript. This study was financially supported in part by JSPS 14208064.

References

Badon-Ghyben, W. (1889), Nota in verband met de voorgenomen putboring nabil Amsterdam, report, 27 pp., Tijdschr. K. Inst. van Ing., Hague, Netherlands.

Bokuniewicz, H. (1980), Groundwater seepage into Great South Bay, New York, *Estuarine Coastal Mar. Sci.*, *10*, 437–444.

Bokuniewicz, H. J. (1992), Analytical descriptions of subaqueous groundwater seepage, *Estuaries*, *15*, 458–464.

Burnett, W. C. (1999), Offshore springs and seeps are focus of working group, *Eos Trans AGU*, *80*, 13–15.

Burnett, W. C., M. Taniguchi, and J. A. Oberdorfer (2001), Measurement and significance of the direct discharge of groundwater into the coastal zone, *J. Sea Res.*, *46*(2), 109–116.

Burnett, W. C., H. Bokuniewicz, M. Huettle, W. S. Moore, and M. Taniguchi (2003), Groundwater and pore water inputs to the coastal zone, *Biogeochemistry*, *66*, 3–33.

Cable, J. E., W. C. Burnett, and J. P. Chanton (1997), Magnitude and variations of groundwater seepage along a Florida marine shoreline, *Biogeochemistry*, *38*, 189–205.

Chanton, J. P., W. C. Burnett, H. Dulaiova, D. R. Corbett, and M. Taniguchi (2003), Seepage rate variability in Florida Bay driven by Atlantic tidal height, *Biogeochemistry*, *66*, 187–202.

Fellows, C. R., and P. L. Brezonik (1980), Seepage flow into Florida lakes, *Water Resour. Bull.*, *16*, 635–641.

Freeze, R. A., and J. A. Cherry (1979), *Groundwater*, 604 pp., Prentice-Hall, Upper Saddle River, N. J.

Gallagher, D. L., A. M. Dietrich, W. G. Reay, M. C. Hayes, and G. M. Simmons Jr. (1996), Ground water discharge of agricultural pesticides and nutrients to estuarine surface water, *Ground Water Monit. Rem.*, *16*(1), 118–129.

Ghyben, W. B. (1899), Notes in verband met voorgenomen put boring Nabji Amsterdam, report, Tijdschr. K. Inst. van Ing., Hague, Netherlands.

Herzberg, A. (1901), Die Wasserversorgung einiger Nordseebader, *J. Gasbeleucht. Wasserversorg.*, *44*, 815–819, 842–844.

Hussain, N., T. M. Church, and G. Kim (1999), Use of ^{222}Rn and ^{226}Ra to trace groundwater discharge into the Chesapeake Bay, *Mar. Chem.*, *65*, 127–134.

Huyakorn, P. S., P. F. Anderson, J. W. Mercer, and H. O. White (1987), Saltwater intrusion in aquifers: Development and testing of a three-dimensional finite element model, *Water Resour. Res.*, *23*, 293–312.

Kim, G., and D. W. Hwang (2002), Tidal pumping of groundwater into the coastal ocean revealed from submarine Rn-222 and CH4 monitoring, *Geophys. Res. Lett.*, *29*(14), 1678, doi:10.1029/2002GL015093.

Krupa, S. L., T. V. Belanger, H. H. Heck, J. T. Brok, and B. J. Jones (1998), Krupaseep—The next generation seepage meter, *J. Coastal Res.*, *25*, 210–213.

Lee, D. R. (1977), A device for measuring seepage flux in lakes and estuaries, *Limnol. Oceanogr.*, *22*, 140–147.

Li, L., D. A. Barry, F. Stagnitti, and J.-Y. Parlange (1999), Submarine groundwater discharge and associated chemical input to a coastal sea, *Water Resour. Res.*, *35*, 3253–3259.

McBride, M. S., and H. O. Pfannkuch (1975), The distribution of seepage within lakebed, *J Res. U. S. Geol. Surv.*, *3*, 505–512.

Moore, W. S. (1996), Large groundwater inputs to coastal waters revealed by ^{226}Ra enrichments, *Nature*, *380*, 612–614.

Paulsen, R. J., C. F. Smith, D. O'Rourke, and T. Wong (2001), Development and evaluation of an ultrasonic ground water seepage meter, *Ground Water*, *39*, 904–911.

Rosenberry, D. O., and R. H. Morin (2004), Use of an electromagnetic seepage meter to investigate temporal variability in lake seepage, *Ground Water*, *42*, 68–77.

Segol, G., and G. F. Pinder (1976), Transient simulation of saltwater intrusion in southeastern Florida, *Water Resour. Res.*, *12*, 65–70.

Shaw, R. D., and E. E. Prepas (1990), Groundwater-lake interactions: II. Nearshore seepage patterns and the contribution of ground water to lakes in central Alberta, *J. Hydrol.*, *119*, 121–136.

Shimada, J., K. Watanabe, M. Taniguchi, K. Miyaoka, and S. Onodera (2003), Behavior of saltwater-freshwater interface due to tidal change observed from high resolution resistivity measurements, paper presented at Fall Meeting, Jpn. Assoc. of Groundwater Hydrol., Tokyo.

Shinn, E. A., C. D. Reich, and T. D. Hickey (2002), Seepage meters and Bernoulli's revenge, *Estuaries*, *25*, 126–132.

Smith, L., and W. Zawadzki (2003), A hydrogeologic model of submarine groundwater discharge: Florida intercomparison experiment, *Biogeochemistry*, *66*, 95–110.

Taniguchi, M. (2002), Tidal effects on submarine groundwater discharge into the ocean, *Geophys. Res. Lett.*, *29*(12), 1561, doi:10.1029/2002GL014987.

Taniguchi, M., and Y. Fukuo (1993), Continuous measurements of groundwater seepage using an automatic seepage meter, *Ground Water*, *31*, 675–679.

Taniguchi, M., and Y. Fukuo (1996), An effect of seiche on groundwater seepage rate into Lake Biwa, Japan, *Water Resour. Res.*, *32*, 333–338.

Taniguchi, M., and H. Iwakawa (2001), Measurements of submarine groundwater discharge rates by a continuous heat-type automated seepage meter in Osaka Bay, Japan, *J. Groundwater Hydrol.*, *43*(4), 271–277.

Taniguchi, M., and H. Iwakawa (2004), Submarine groundwater discharge in Osaka Bay, Japan, *Limnology*, *5*, 25–32.

Taniguchi, M., W. C. Burnett, J. E. Cable, and J. V. Turner (2002), Investigation of submarine groundwater discharge, *Hydrol. Processes*, *16*, 2115–2129.

Taniguchi, M., W. C. Burnett, J. E. Cable, and J. V. Turner (2003a), Assessment methodologies of submarine groundwater discharge, in *Land and Marine Hydrogeology*, edited by M. Taniguchi, K. Wang, and T. Gamo, pp. 1–23, Elsevier, New York.

Taniguchi, M., W. C. Burnett, C. F. Smith, R. J. Paulsen, D. O'Rourke, S. L. Krupa, and J. L. Christoff (2003b), Spatial and temporal distributions of submarine groundwater discharge rates obtained from various types of seepage meters at a site in the Northeastern Gulf of Mexico, *Biogeochemistry*, *66*, 35–53.

T. Ishitobi, Nara University of Education, Takabatake, 630-8528, Japan. (a038508@student.nara-edu.ac.jp)

J. Shimada, Department of Earth Sciences, Kumamoto University, 2-39-1, Kurokami, Japan. (jshimada@sci.kumamoto-u.ac.jp)

M. Taniguchi, Research Institute for Humanity and Nature, 335 Takashima-cho, Kamigyo-ku, Kyoto 602-0878, Japan. (makoto@chikyu.ac.jp)